Appl Phys B (2011) 105:421–425
DOI 10.1007/s00340-011-4719-5

**Applied Physics B**
**Lasers and Optics**

# Precise measurement of Brillouin scattering spectrum in the ocean using F–P etalon and ICCD

**K. Liang · Y. Ma · J. Huang · H. Li · Y. Yu**

Received: 23 November 2010 / Revised version: 26 July 2011 / Published online: 11 September 2011


**Abstract** A new method for analyzing the signal of the spectrum of Brillouin scattering in the ocean using F–P etalon and ICCD is proposed. It is based on the principle of interference of the F–P etalon. The capability of the method is confirmed by processing experimental data from stimulated Brillouin scattering spectrum in the water at different temperatures. The experimental results show very good agreement with theoretical values. This method provides a feasible way to measure Brillouin frequency shift and line width with high precision.

## 1 Introduction

The Brillouin lidar system has been proved very useful in remote sensing of the ocean [1–5]. It can be used to measure temperature, sound speed and bulk viscosity of seawater [6, 7]. Among current methods for Brillouin signal measurement, the edge technique [8, 9] cannot obtain the scattering spectrum; the scanning Fabry–Pérot (F–P) interferometer [10, 11] requires long scanning time, therefore they have limited applications. The F–P etalon combined with ICCD [12] can overcome this problem and has more capability in remote sensing applications.

K. Liang · Y. Ma · J. Huang (✉) · H. Li · Y. Yu
Department of Electronics and Information Engineering,
Huazhong University of Science and Technology, Wuhan 430074,
P.R. China
e-mail: junhuang@smail.hust.edu.cn
Fax: +86-27-87556304

K. Liang · Y. Ma · J. Huang · H. Li · Y. Yu
Wuhan National Laboratory for Optoelectronics, Wuhan 430074,
P.R. China

The information obtained using F–P etalon and ICCD provides a Brillouin scattering spectrum based on interference rather than absorption. Current technique measures frequency shift plainly based on the relationship between peak positions of different orders [12]. Unfortunately, this method does not take full advantage of other information provided by the interference spectrum such as intensities. So application of this method is limited to frequency shift measurement. In order to determine more seawater features in ocean remote sensing, it is crucial to obtain multi parameters of Brillouin scattering besides frequency shift.

The aim of this paper is to obtain a precise Brillouin spectrum from interference fringe pattern so that more features can be measured. This novel spectrum signal processing method is helpful for rapid multi parameters remote sensing in the ocean, making the Brillouin lidar system using F–P etalon and ICCD a more capable technology.

## 2 Theoretical considerations

In brief, the backscattered Brillouin echo signal collected by a telescope is transmitted through F–P etalon and displayed as fringes on ICCD, as shown in Fig. 1. The fringe intensity pattern is a function of the Brillouin spectrum and the F–P etalon transmission function. Ideally the transmission function of F–P etalon is called an Airy function and is expressed as [13]

$$A(\lambda, r) = \frac{1}{1 + F \times \sin^2(\frac{2\pi\mu d}{\lambda}\cos\theta_t)} \tag{1}$$

where $\mu$ is refractive index, $d$ is the plate spacing of F–P etalon, $\lambda$ is the wavelength of incident light, $\theta_t$ is the refraction angle of incident light and is expressed by focusing

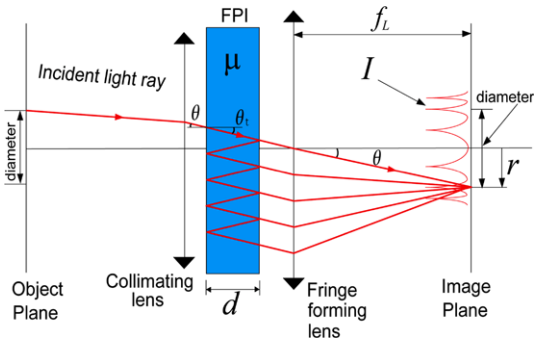


**Fig. 1** Schematic of a F–P etalon

focal length $f_L$, image radius $r$ and refractive index $\mu$ in the following way:

$$\theta_t = \sin^{-1}\left(\frac{r}{\sqrt{f_L^2 + r^2 \times \mu}}\right) \tag{2}$$

$F$ is the coefficient of finesse and is expressed by surface reflectance $R$:

$$F = \frac{4R}{(1-R)^2} \tag{3}$$

It can be concluded from the form of the Airy function that $m$th order constructive interference occurs when $\frac{2\pi\mu d}{\lambda}\cos\theta_t = m\pi$ as the transmittance reaches its maximum value. For incident light with single frequency, as the fringe radius $r$ increases, $\theta_t$ will also increase, causing $\cos\theta_t$ to decrease, therefore constructive interference will occur several more times with less number of orders. As a result, the interference fringes appear as a group of concentric circles with different radii, varying as the incident frequency changes.

When incident light with various frequencies transmits through an F–P etalon, the intensity observed with ICCD at a certain radius $r$ should be the sum of all intensities contributed by each single frequency, and is expressed as [13]

$$I(r) = \frac{GA_0\Omega TQ}{4\pi}\int_{-\infty}^{+\infty} S(\nu)\times T_{\mathrm{F}}(\nu)\times A\left(\frac{c}{\nu}, r\right)d\nu + I_{\mathrm{B}} \tag{4}$$

Here $G$ is the gain factor of the receiving optical path and ICCD, $A_0$ is the area of the etalon, $\Omega$ is the solid angle, $T$ is the integration time, $Q$ is the quantum efficiency of the ICCD, $\nu$ is the frequency of light, $S(\nu)$ represents the incident spectrum, $T_{\mathrm{F}}(\nu)$ is the transmittance function of front-end optical system, $c$ is velocity of light in vacuum, $A(\frac{c}{\nu}, r)$ is the above mentioned Airy function ($\lambda = \frac{c}{\nu}$), $I_{\mathrm{B}}$ represents the background noise.

In reality, the laser used in experiment is influenced by lidar system and optical system, the incident laser does not carry a single frequency, instead it is broadened by instrument. After instrument broadening, the incident spectrum $S(\nu)$ is expressed as

$$\begin{aligned} S(\nu) &= \int_{-\infty}^{+\infty} B(\omega)\times D_{\mathrm{I}}(\nu-\omega)\,d\omega \\ &= \int_{-\infty}^{+\infty} B(\omega)\times\frac{2\sqrt{\ln 2}\times A}{\sqrt{\pi}\times\Delta\nu_G} \\ &\quad\times\exp\left\{\frac{-4\ln 2\times(\nu-\omega)^2}{\Delta\nu_G^2}\right\}d\omega \end{aligned} \tag{5}$$

where $D_{\mathrm{I}}(\nu)$ is the instrument broadening function, generally it is considered to be a Gaussian function with line width (FWHM) $\Delta\nu_G$ and normalization constant $A$. $B(\nu)$ is the Brillouin scattering spectrum stimulated by laser of a single frequency $\nu$, it is a Lorentzian function which is expressed as

$$B(\nu) = B\times\frac{2}{\pi}\times\frac{\Gamma_{\mathrm{B}}}{4(\nu-\nu_{\mathrm{B}})^2+\Gamma_{\mathrm{B}}^2} \tag{6}$$

$\Gamma_{\mathrm{B}}$ is the line width of Brillouin spectrum, $\nu_{\mathrm{B}}$ is the frequency shift, $B$ is normalization constant. The shape of a Brillouin spectrum is uniquely determined by $\Gamma_{\mathrm{B}}$ and $\nu_{\mathrm{B}}$.

When $\upsilon$ changes slightly, $T_{\mathrm{F}}(\nu)$ can be approximately seen as a constant $T_{\mathrm{F}}|_\nu$. As the line width of instrumental broadening $\Delta\nu_G$ is extremely small, so instrument broadening function $D_{\mathrm{I}}(\nu)$ can be simplified as impulse function $\delta(\nu-\tau)$. Thus (5) can be expressed as

$$\begin{aligned} S(\nu) &= \int_{-\infty}^{+\infty} B(\omega)\times D_{\mathrm{I}}(\nu-\omega)\,d\omega \\ &\approx \int_{-\infty}^{+\infty} B(\omega)\times\delta(\nu-\omega)\,d\omega = B(\nu) \end{aligned} \tag{7}$$

Taken this into consideration, (4) can be simplified as

$$I'(r) = I(r) - I_{\mathrm{B}} = K\int_{-\infty}^{+\infty} B(\nu)\times A\left(\frac{c}{\nu}, r\right)d\nu \tag{8}$$

where

$$K = \frac{GA_0\Omega TQT_{\mathrm{F}}|_\nu}{4\pi} \tag{9}$$

$I'(r)$ stands for the denoised fringe intensity after elimination of background noise. It is the integration of Brillouin spectrum and Airy function. In the experiment $A(\frac{c}{\nu}, r)$ is determined by F–P etalon, and $I'(r)$ can be obtained; therefore Brillouin scattering spectrum $B(\nu)$ can be acquired by a nonlinear fitting.

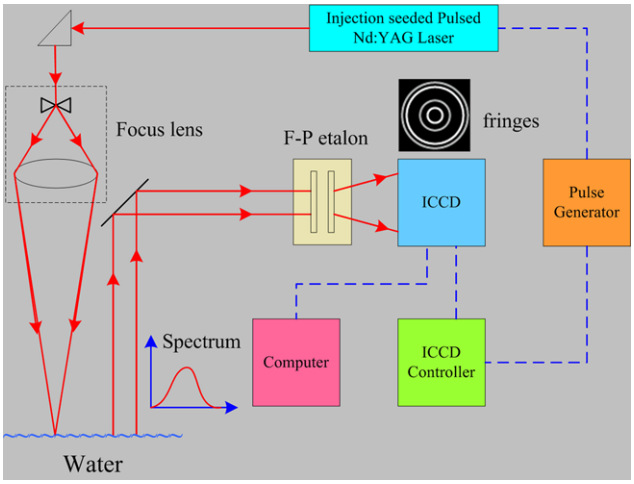


**Fig. 2** Schematic diagram of a Brillouin lidar system

## 3 Experiments

### 3.1 Experimental configuration

Figure 2 shows the configuration of the Brillouin lidar system using the F–P etalon and ICCD. In order to increase the detected depth and resolution, a lidar system based on stimulated Brillouin scattering [14] was used. Specifically, a focus lens system was added to the optical path so that the laser beam can concentrate at a certain depth where the stimulated Brillouin scattering is generated. The stimulated Brillouin scattering signal was first collected by optical system and then transmitted through F–P etalon, the interference fringes were recorded by ICCD and eventually sent to PC for analysis to obtain the Brillouin spectrum.

The focus lens system consists of a small diverging lens and a large converging lens, the laser beam is first diverged and propagate in water through longer distance and then converged to excite the stimulated Brillouin scattering, therefore the detection depth is increased. The experimental results show that the detection can reach 7–9 attenuation lengths, which is 58.3–75.0 meters as the attenuation coefficient of clean water used in experiment was 0.12.

The calibration of F–P etalon should be performed to obtain an accurate measurement. In the experiment the F–P etalon was calibrated using a stable He-Ne laser. The laser has two longitudinal modes, their frequency difference is the longitudinal mode spacing $\Delta\nu$. When lasers of the two longitudinal modes pass through an F–P etalon, fringe patterns can be observed on ICCD, as shown in Fig. 3. For each order of fringes, the inner ring corresponds to longitudinal mode with lower frequency, and the outer ring stands for longitudinal mode with higher frequency. $r_1$ and $r_2$ are the radius of 1st and 2nd order of the inner peaks, $r_1'$ is the radius of the 1st order of the outer peak. According to interference

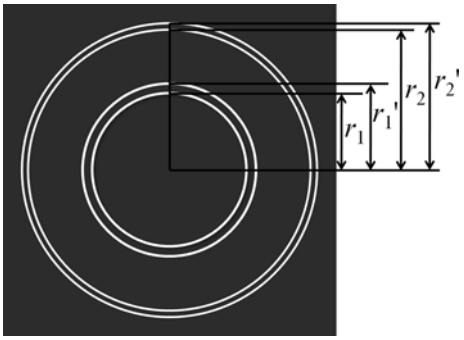


**Fig. 3** Schematic of fringe pattern of incident lights with two frequencies

theories [7], the FSR (free spectral range) can be expressed as

$$\mathrm{FSR} = \frac{r_2^2 - r_1^2}{r_1'^2 - r_1^2}\Delta\nu \tag{10}$$

The real FSR of a given F–P etalon can be determined by this equation. In our experiment, The F–P etalon used was a CVI solid etalon made of quartz with a free spectral range of FSR = 20 GHz and a reflective rate of 99.5%. After calibration, the FSR was calibrated to 19.6 GHz.

As the Brillouin scattering spectrum has small frequency shift and line width, the laser used was an stable injection-seeded pulsed Nd:YAG laser (Continuum Powerlite Precision II 8000) with a wavelength of 532 nm, a pulse energy of 650 mJ, a repetition rate of 10 Hz and a line with of 0.003 $\mathrm{cm}^{-1}$ (90 MHz).

The ICCD system consisted of an ICCD camera and an ICCD controller, The ICCD camera used was Princeton Instruments PI-MAX II with a resolution of 1024 × 256, a pixel size of 26 × 26 μm and a minimum gate width of 2ns. The ICCD controller used was Princeton Instruments ST-133. Stanford Research System's DG535 was also used to synchronize the laser with the ICCD system.

### 3.2 Obtaining Brillouin scattering spectrum

The F–P interference fringes of fresh water (0‰ salinity, measured at 1 m depth) of different temperatures were recorded by the above mentioned lidar system.

In the experiment, there are only Stokes lines and no anti-Stokes lines in the SBS spectrum. The fringe pattern obtained is similar to Fig. 3, the outer ring represents the Rayleigh scattering, and the inner ring represents the Brillouin scattering. Figure 4 shows the interference spectrum with temperature at 25°C and salinity of 0‰, it was processed from the original fringe pattern with de-noising, smoothing and data selection algorithms. As discussed in theoretical considerations, the normalized intensity values on the spectrum should fit with the function expressed in (8).

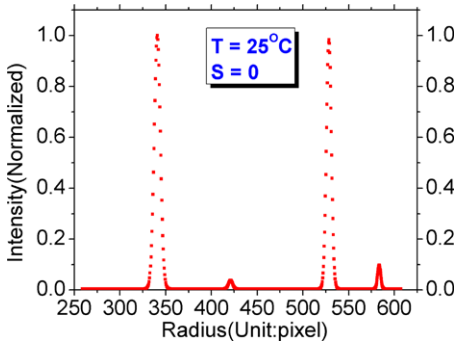


**Fig. 4** Radial slice of fringes

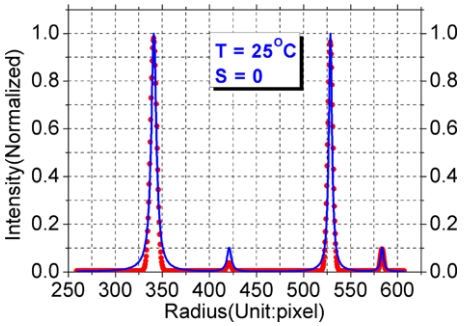


**Fig. 5** Radial slice of fringes and the fitting curve

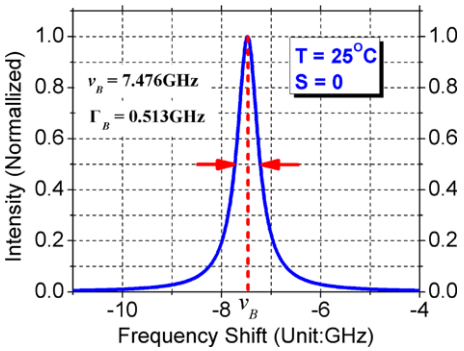


**Fig. 6** Retrieved Brillouin spectrum

A Levenberg–Marquardt algorithm was employed to provide a nonlinear least-square fit to the data of the spectrum. The uncertainties were determined by the 95% confidential interval calculated by Jacobian Matrix in the algorithm. The fitted curve obtained is shown in Fig. 5. The red dots on the figure represent samples taken from interference fringes, the blue solid line is the optimal fitted curve, which fits well with the original values. Based on the fitted interference pattern, the actual stimulated Brillouin scattering spectrum was retrieved, as shown in Fig. 6. According to the retrieved spectrum with temperature of 25°C and salinity of 0‰, the measured Brillouin frequency shift was $7.476 \pm 0.003$ GHz, the measured line width was $0.513 \pm 0.018$ GHz.

**Table 1** Analysis of fitted curves at various temperatures

| Temperature (°C ) | Corrcoef | Uncertainty (Brillouin frequency shift) | Uncertainty (line width) |
|---|---|---|---|
| 10 | 0.9878 | ±6 MHz | ±36 MHz |
| 15 | 0.9888 | ±6 MHz | ±17 MHz |
| 20 | 0.9880 | ±3 MHz | ±18 MHz |
| 25 | 0.9876 | ±3 MHz | ±18 MHz |

### 3.3 Experimental results and discussions

The capability of the proposed method can be confirmed by fitted error analysis and comparison with theoretical values.

Table 1 shows the correlation coefficient and uncertainty of the fitted curves at different temperatures. The correlation coefficient indicates that the fitted curve (blue line) showed good agreement with experimental data (red dot). However, data points around the peak are larger than the fitted values while data points near the base are lower than the fitted values. The errors here should be caused by ignoring instrument broadening in the fitting function. As we plan to take this into consideration in the future, the fitted curves would hopefully be more precise.

Precision in measurements are limited by pixel size and resolution of ICCD, considering a gain in resolution by means of image processing and fitting procedure, the overall measured uncertainty is reduced. The uncertainties in the measurement of the Brillouin frequency shift and line width are shown in Table 1.

When the salinity is 0, an uncertainty in Brillouin shift measurement of 1 MHz corresponds to a temperature resolution of 0.04°C [15], and an uncertainty in Brillouin line width measurement of 1 MHz would lead to uncertainty of 0.017°C [16]. So an overall Brillouin shift uncertainty of ±3∼6 MHz will result in an uncertainty of 0.12∼0.24°C in temperature, and an line width uncertainty of ±17∼36 MHz will result in 0.29∼0.61°C uncertainty in temperature.

Table 2 and Table 3 show comparison between measured values and theoretical values [11, 17] of Brillouin scattering frequency shift and line width of fresh water at various temperatures. For frequency shift, the error at 10°C was greater, with an absolute error of 0.224 GHz and a relative error of 3.08%, while errors at other temperatures were extremely small, with absolute errors of 0.027 GHz–0.07 GHz and relative errors of 0.36%–0.95%. Similar results occur in the line width: at 10°C the error was greater with an absolute error of 0.032 GHz and a relative error of 3.53%; at other temperatures, the absolute errors were 0.001 GHz–0.032 GHz, the relative errors were 0.14%–0.86%.

It can be concluded from Table 2 and Table 3 that measured values agreed quite well with theoretical values with extremely small error, except for values at 10°C . The reason why a greater uncertainty was observed at 10°C should

**Table 2** Analysis of errors between measured ($\nu_B$) and theoretical ($\nu_{B'}$) values of frequency shift

| Temperature (°C ) | $\nu_B$ (GHz) | $\nu_{B'}$ (GHz) | error (GHz) | relative |
|---|---|---|---|---|
| 10 | 7.040 | 7.264 | 0.224 | 3.08% |
| 15 | 7.426 | 7.356 | 0.07 | 0.95% |
| 20 | 7.409 | 7.436 | 0.027 | 0.36% |
| 25 | 7.476 | 7.507 | 0.031 | 0.41% |

**Table 3** Analysis of errors between measured ($\Gamma_B$) and theoretical ($\Gamma_{B'}$) values of line width

| Temperature (°C ) | $\Gamma_B$ (GHz) | $\Gamma_{B'}$ (GHz) | error (GHz) | relative |
|---|---|---|---|---|
| 10 | 0.936 | 0.904 | 0.032 | 3.53% |
| 15 | 0.705 | 0.704 | 0.001 | 0.14% |
| 20 | 0.579 | 0.584 | 0.005 | 0.86% |
| 25 | 0.513 | 0.512 | 0.001 | 0.19% |

be that there were fewer samples available. The number of pixels effectively recorded by ICCD in an experiment is determined by power of the laser as well as transverse mode of the laser pulse. The transverse mode at 10°C measurement might not be as good as those at other temperatures, and as a result the power received by ICCD was relatively low and available points were reduced.

In order to increase the precision of the measured Brillouin spectrum, several improvements will be implemented in the future. First, the error will be reduced by enlarging the focal length of lens in the optical system, so interference pattern of each order would be larger and cover more pixels. In addition, instrument broadening of lidar system and pixel size of ICCD were two major source of measurement error. The instrument broadening was very small but not ignorable, as it caused deviations on values of fringes, which would be more significant for lower values. We plan to analyze this impact in the future to minimize error. On the other hand, pixel size of ICCD determines its minimum resolution. Smaller pixel size means better resolution and less error. If the $26 \times 26$ μm sized ICCD in the experiment was replaced by ICCD with smaller pixel size like $13 \times 13$ μm, less error would also be observed.

## 4 Conclusion

In summary, a method for precise measurement of Brillouin scattering spectrum in the ocean using F–P etalon and ICCD was proposed. This method takes full advantage of position and intensity information on F–P interference pattern to obtain a precise spectrum. It measures parameters including frequency shift and line width of the spectrum at the same time and can make significant contribution to rapid multi parameter sensing in the ocean.

**Acknowledgements** The authors would like to thank National Natural Science Foundation of China (grant No. 61078062 and grant No. 61108074) and Research Fund for the Doctoral Program of Higher Education of China (grant No. 20100142120012). Also, the authors would like to thank Prof. D. Liu for provision of experimental data and his helpful discussions.

## References

1. J.G. Hirschberg, J.D. Byrne, A.W. Wouters, C. George, Appl. Opt. **23**, 2624 (1984)
2. G.D. Hickman, J.M. Harding, M. Carnes, A. Pressman, G.W. Kattwar, E.S. Fry, Remote Sens. Environ. **36**, 165 (1991)
3. D.A. Leonard, H.E. Sweeney, Proc. SPIE **1302**, 568 (1990)
4. A. Popescu, K. Schorstein, T. Walther, Appl. Phys. B **79**, 955 (2004)
5. J. Shi, X. Chen, M. Ouyang, W. Gong, J. Liu, D. Liu, Appl. Phys. B, Lasers Opt. **95**, 657 (2009)
6. Y.E. Emery, E.S. Fry, Proc. SPIE **2963**, 210 (1997)
7. M. Ouyang, J. Shi, L. Zhaoi, X. Chen, H. Jing, Appl. Phys. B **91**, 381 (2008)
8. C.L. Korb, B.M. Gentry, C. Weng, Appl. Opt. **31**, 4202 (1992)
9. P. Piironen, E.W. Eloranta, Opt. Lett. **19**, 234 (1994)
10. D. Liu, J. Xu, R. Li, R. Dai, W. Gong, Opt. Commun. **203**, 335 (2002)
11. J. Xu, X. Ren, W. Gong, R. Dai, D. Liu, Appl. Opt. **42**, 6704 (2003)
12. J. Shi, G. Li, W. Gong, J. Bai, Y. Huang, Y. Liu, S. Li, D. Liu, Appl. Phys. B **90**, 569 (2008)
13. H. Nakajima, S. Okano, H. Fukunishi, T. Ono, Appl. Opt. **34**, 8382 (1995)
14. J. Shi, M. Ouyang, W. Gong, S. Li, D. Liu, Appl. Phys. B **86**, 177 (2007)
15. K. Schorstein, A. Popescu, M. Gobel, T. Walther, Sensors **8**, 5820 (2008)
16. W. Gao, Z. Lv, Y. Dong, W. He, Chin. Opt. Lett. **4**, 428 (2006)
17. E.S. Fry, Y. Emery, X. Quan, J.W. Katz, Appl. Opt. **36**, 6887 (1997)